Influence of the Structural Properties of Poly(vinylidene fluoride) Membranes on the Heterogeneous Nucleation Rate of Protein Crystals

Efrem Curcio,*,†,‡ Enrica Fontananova,†,‡ Gianluca Di Profio,†,‡ and Enrico Drioli†,‡

Department of Chemical Engineering and Materials, University of Calabria, Via P. Bucci, CUBO 45/A, I-87030, Arcavacata di Rende (CS), Italy, and Institute on Membrane Technology (ITM-CNR), c/o University of Calabria, Via P. Bucci, CUBO 17/C, I-87030, Arcavacata di Rende (CS), Italy

Received: March 13, 2006; In Final Form: April 30, 2006

In this study, the influence of the morphological parameters of microporous poly(vinylidene fluoride) (PVDF) membranes on the heterogeneous nucleation rate of hen egg white lysozyme (HEWL) crystals has been investigated. Experiments have been carried out on membranes prepared by non-solvent-induced phase inversion method, using PVDF-*co*-hexafluoropropylene (Kynarflex 2800) and PVDF homopolymer (Kinar 460), and adding LiCl and poly(vinylpyrrolidone) (PVP) in order to modulate the pore structure. From a theoretical point of view, the free Gibbs energy balance for the formation of a critical nucleus has been adapted to nonporous surfaces, thus obtaining a mathematical correlation between the energy nucleation barrier, the membrane porosity, and the contact angle between protein solution and polymeric substrate. The energetic barrier to heterogeneous nucleation was found to increase at higher contact angles—according to the prediction of classical theory—and to decrease at higher porosity. For instance, the predicted $\Delta G_{het}/\Delta G_{hom}$ ratio for PVDF−Kynarflex (PVP 2.5%) membrane with porosity of 0.11 was 0.30, 35% lower with respect to the value calculated by the Volmer equation for a dense polymeric matrix having the same contact angle (87.4 ± 5.8°). In addition, the effect of the membrane pore size, porosity, and thickness on the removal rate of solvent have been discussed. For example, the transmembrane flux through PVDF−Kynar (LiCl 5.0%) membrane was 12% inferior than the one measured under the same experimental conditions through PVDF−Kynarflex (LiCl 7.5%) membrane, the latter having similar pore size and thickness but higher porosity (0.44 vs 0.32). The possibility to achieve rapidly a high level of supersaturation is expected to increase the nucleation rate. In general, measurements performed during crystallization tests carried out at pH 4.5 in NaAc 0.05 M buffer with different precipitant (NaCl) concentrations agree with the predicted trends.

Introduction

Protein crystallization methodologies aiming to promote heterogeneous nucleation have increased their significance in recent years. It is well recognized that the presence of a solid substrate may improve nucleation rate through the combination of different aspects: modification of the supersaturation profile near the surface due to concentration polarization; template effects due to adsorption of solutes at the surface; influence of surface characteristics leading to specific interactions with the solute. Some exploratory investigations aiming to emphasize or elucidate these aspects are reported in the literature. The effect of mineral substrates (including apophyllite, topaz, lepidolite, magnetite and galena), on hen egg white lysozyme (HEWL) nucleation rate has been the object of research for the past 20 years.[1,2]

More recently, polymeric films containing ionizable groups, such as sulfonated polystyrene, cross-linked gelatin films with adsorbed poly-L-lysine or entrapped poly-L-aspartate, and silk fibroin with entrapped poly-L-lysine or poly-L-aspartate, have been investigated for HEWL and concanavalin A.[3,4]

Microarrayed multiple cell silicon devices were proposed by Sanjoh and colleagues with the aim to activate heterogeneous nucleation/crystallization of HEWL.[5,6] In general, approaches addressed to promote heterogeneous nucleation provide interesting results in terms of shorter induction times and accelerated nucleation rates of protein crystals with respect to those reported by using traditional methods.

All this experimental evidence is theoretically supported by the thermodynamic model elaborated by Volmer almost 80 years ago.[7] Free energy for critical nucleus formation, given by the difference between the energy gained upon formation of a bulk phase and the energy required to form new surface area, is a crucial parameter in nucleation theory. In particular, the energy balance includes positive contributions of interfacial free energies of the nucleus−liquid (γ_L) and nucleus−substrate (γ_i) interfaces, and a negative contribution for the liquid−substrate (γ_S) interface that is displaced.[8]

The traditional approach is to use Young's equation (for smooth, perfectly planar, and chemically homogeneous surfaces) in order to relate these three interfacial free energies to the contact angle (θ) between solution and substrate.

According to Volmer, the free energy of formation, ΔG_{het}, of a nucleus of critical size on a solid surface is given by

$$\frac{\Delta G_{het}}{\Delta G_{hom}} = \left(\frac{1}{2} - \frac{3}{4}\cos\theta + \frac{1}{4}\cos^3\theta\right) \quad (1)$$

where ΔG_{hom} refers to the case of homogeneous nucleation.

* Corresponding author.
† University of Calabria.
‡ Institute on Membrane Technology.

10.1021/jp061531y CCC: $33.50
Published on Web 06/03/2006

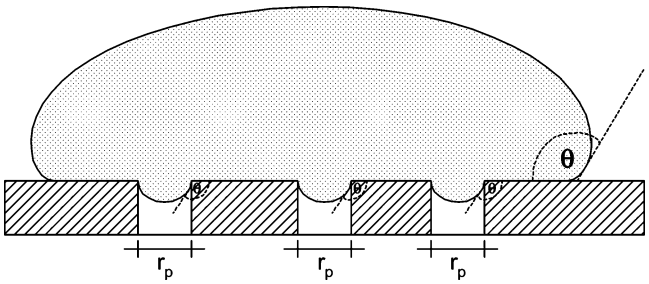

Figure 1. Definition of the contact angle θ between the heterogeneous surface and the crystallizing solution.

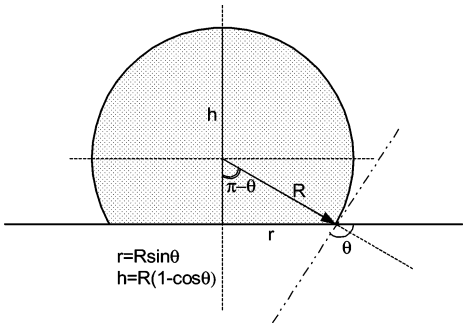

Figure 2. Geometry of a sphere cap related to the shape of a drop on the membrane surface. θ is the contact angle at the three-phase line.

In addition to previously mentioned techniques, also microporous hydrophobic membranes have been recently used for protein crystallization purposes.[9] In a membrane-based crystallization device, polymeric membranes (i) generate supersaturation by transferring the vaporized solvent from the protein solution to an hypertonic salt solution, under a partial pressure gradient, and (ii) promote heterogeneous nucleation.

The effectiveness of this method has been demonstrated in terms of accelerated crystallization kinetics[10,11] and fine control of the crystal shape and morphology.[12,13]

The traditional approach of nucleation states that interactions between charged proteins and substrate can produce a sufficiently large difference in surface free energy that improves crystallization rate; on the other hand, experimental tests carried out on porous silicon show that the kinetics enhancement occurs independently of the charge sign of macromolecules.[14] A theoretical explanation for this evidence is suggested in this work.

When porous materials (membranes) are used, eq 1 becomes not applicable since it is based on Young's equation that is strictly valid for ideal and nonporous surfaces. For nonideal (porous) surfaces, a modified form of the Young equation that connects surface porosity, measured contact angle, and equilibrium contact angle has been derived by Troger and colleagues and successfully tested on microporous poly(tetrafluoroethylene) membranes.[15]

On this basis, the purpose of this paper is to derive theoretically the value of free energy barrier for heterogeneous nucleation process—activated by a porous membrane—as a function of porosity (ϵ) and contact angle (θ) between the mother solution and the solid substrate (an exemplification of the system is given in Figure 1).

To verify the connection between theory and experiments, and to elucidate the design principles of a membrane crystallizer, nucleation rate measurements have been carried out on microporous hydrophobic poly(vinylidene fluoride) (PVDF) membranes having different morphologies and structural properties.

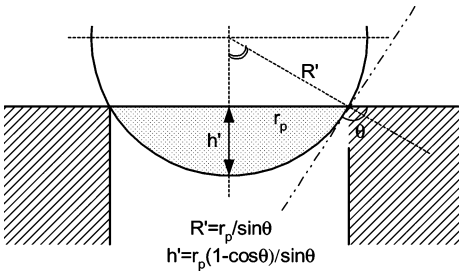

Figure 3. Geometry of a sphere cap related to the shape of a drop inside a pore of the membrane. θ is assumed to be equal to the contact angle at the three-phase line.

PVDF was employed as biomaterial due to its nontoxicity, high durability, and chemical stability. Porous polymeric substrates were prepared in the form of flat-sheet membranes by a nonsolvent-induced phase inversion method, according to procedures illustrated in Materials and Methods.

Theory

Solution drops deposited on a porous membrane were assumed with spherical cap shape (Figure 2), R, r, and h being the main radius, the contact radius, and the height of the drop, respectively.

Geometrical relations give

$$A_{SL} = \pi r^2 = \pi R^2 \sin^2 \theta \tag{2}$$

$$A_L = 2\pi Rh = 2\pi R^2(1 - \cos \theta) \tag{3}$$

$$V = \pi h^2\left(R - \frac{h}{3}\right) = \pi \frac{R^3}{3}(1 - \cos \theta)^2(2 + \cos \theta) \tag{4}$$

where A_{SL} is the solid−liquid interfacial area generated by drop formation, A_L is the surface area of the liquid sessile drop, and V the volume of the droplet cap.

Droplets occupy partially the pores of the membrane, and therefore, the related surfaces and volumes have to be taken into account. If r_p is the pore radius (refer to Figure 3 for the meaning of the additional geometric parameters)

$$A_{SL} = \pi {r_p}^2 \tag{2'}$$

$$A_L = 2\pi R'h' = 2\pi\left(\frac{r_p}{\sin \theta}\right)^2(1 + \cos \theta) \tag{3'}$$

$$V = \pi h'^2\left(R' - \frac{h'}{3}\right) = \pi \frac{{r_p}^3}{3}\frac{(1 + \cos \theta)^2(2 - \cos \theta)}{\sin^3 \theta} \tag{4'}$$

where A_{SL}', A_{SL}', and V are the pore surface, the area, and the volume of the portion of droplet that penetrates into the pore.

For a porous structure, the surface porosity ϵ is defined as the ratio of the total pore areas ($\sum A_p$) on the whole geometrical surface A of the membrane. The number of pores n_p covered by the surface area of the sessile drop contacting the solid substrate is

$$n_p = \epsilon \frac{R^2}{{r_p}^2} \sin^2 \theta \tag{5}$$

It is physically reasonable to assume that the contact angles on the three-phase lines are equal both on the outer drop border and over the pores (Figure 1).

The overall volume (n_pV') of the sphere caps into the pores is

$$n_pV' = \frac{\pi}{3}\epsilon r_p R^2 \frac{(1+\cos\theta)^2(2-\cos\theta)}{\sin\theta} = \frac{\pi}{3}\epsilon\alpha R^3(1+\cos\theta)^2(2-\cos\theta) \quad (6)$$

where

$$\alpha = \frac{r_p}{R\sin\theta} \quad (6')$$

The total free energy change due to the formation of a spherical cap droplet of a crystal on a porous support includes both volumetric and surface terms

$$\Delta G_{het} = -\frac{\pi R^3}{3}\frac{\Delta\mu}{\Omega}(1-\cos\theta)^2(2+\cos\theta) - \frac{\pi}{3}r_p R^2\frac{\Delta\mu}{\Omega}\frac{(1+\cos\theta)^2(2-\cos\theta)}{\sin\theta} + 2\pi R^2\gamma_L[(1-\cos\theta)+\epsilon(1+\cos\theta)] - \pi R^2(\gamma_S-\gamma_i)(1-\epsilon)\sin^2\theta \quad (7)$$

where Ω is the molar volume, and

$$\Delta\mu \approx kT\ln\frac{c}{c^*} \quad (7')$$

being $\Delta\mu$ the variation of chemical potential, k the Boltzmann's constant, T the absolute temperature, c the actual concentration, and c^* the equilibrium concentration (saturation).

Considering the mechanical equilibrium condition for a nonwetting liquid drop on a porous structure, the modified version of the Young equation derived by Tröger[15] gives

$$(\gamma_S-\gamma_i) = \gamma_L\left(\cos\theta + \frac{4\epsilon(1+\cos\theta)}{(1-\epsilon)(1-\cos\theta)}\right) \quad (8)$$

After substitution of eq 8 in the last term of eq 7, the condition of minimum to the variation of the free Gibbs energy has been imposed

$$\frac{\partial\Delta G_{het}}{\partial R} = 0 \quad (9)$$

The radius R^* of a critical cluster nucleated on a surface of a porous substrate is, therefore

$$R^* = \frac{2\gamma_L\Omega}{\Delta\mu}\{\{[2(1-\cos\theta)-\sin^2\theta\cos\theta] + \epsilon[2(1+\cos\theta)+\sin^2\theta\cos\theta-4(1+\cos\theta)^2]\}/[(1-\cos\theta)^2(2+\cos\theta)+\alpha\epsilon(1+\cos\theta)^2(2-\cos\theta)]\} \quad (10)$$

For $\epsilon = 1$ and $\theta = 180°$, the value of R^* becomes identical to the one found for homogeneous nucleation; this is the same predicted by classical theory of heterogeneous nucleation occurring on a nonporous surface ($\epsilon = 0$).

For a critical cluster nucleating in the homogeneous phase

$$\Delta G^*_{hom} = \frac{16}{3}\pi\gamma_L{}^3\left(\frac{\Omega}{\Delta\mu}\right)^2 \quad (11)$$

being ΔG^*_{hom} the value of the Gibbs energy threshold for homogeneous nucleation. In the limiting situation of $\alpha = 0$, the volumetric contribution of droplets into pores becomes null in eq 7; in this case, simplification of trigonometric terms in eq 10 gives rise to a formula simpler to handle

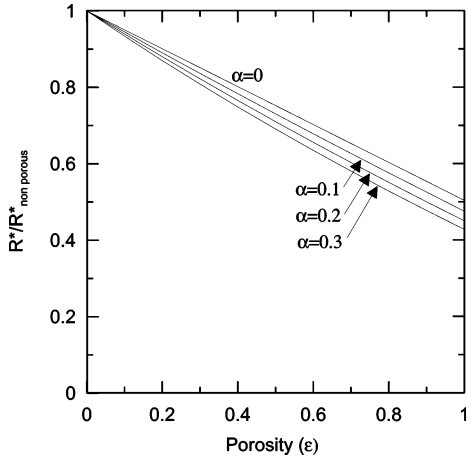

Figure 4. Ratio between the value of critical radius R* (from eq 10) at different α, and the value of the critical radius $R^*_{nonporous}$ for a dense support (from eq 12′).

$$R^* = \frac{2\gamma_L\Omega}{\Delta\mu}\left[1-\epsilon\frac{(1+\cos\theta)^2}{(1-\cos\theta)^2}\right] \quad (12)$$

For $\epsilon = 0$, eq 12 reduces to the classical value given by Volmer theory for a nonporous substrate

$$R^*_{nonporous} = \frac{2\gamma_L\Omega}{\Delta\mu} \quad (12')$$

In Figure 4, the ratio between R^* (evaluated by eq 10) and $R^*_{nonporous}$ (from eq 12′) is plotted versus porosity at different values of α and for a measured contact angle of 100°. This diagram suggests that the negligibility of droplets volume into pores is reasonable (error within 10%) for crystals at least three times larger than the membrane pore size or for membranes with moderate porosity.

To calculate the energetic barrier to heterogeneous nucleation occurring on a porous membrane, eq 12 is substituted in eq 7

$$\Delta G^*_{het} = -\frac{\pi}{3}\frac{\Delta\mu}{\Omega}\left(\frac{2\gamma_L\Omega}{\Delta\mu}\right)^3\left[1-\epsilon\frac{(1+\cos\theta)^2}{(1-\cos\theta)^2}\right]^3(1-\cos\theta)^2(2+\cos\theta) + \ldots + 2\pi\gamma_L\left(\frac{2\gamma_L\Omega}{\Delta\mu}\right)^2\left[1-\epsilon\frac{(1+\cos\theta)^2}{(1-\cos\theta)^2}\right][(1-\cos\theta)+\epsilon(1+\cos\theta)] + \ldots - \pi\gamma_L\left(\frac{2\gamma_L\Omega}{\Delta\mu}\right)^2\left[1-\epsilon\frac{(1+\cos\theta)^2}{(1-\cos\theta)^2}\right]^2[(1-\epsilon)\sin^2\theta\cos\theta + 4\epsilon(1+\cos\theta)^2] \quad (13)$$

Dividing eq 13 by eq 11, with appropriate simplifications

$$\frac{\Delta G^*_{het}}{\Delta G^*_{hom}} = \frac{1}{4}(2+\cos\theta)(1-\cos\theta)^2\left[1-\epsilon\frac{(1+\cos\theta)^2}{(1-\cos\theta)^2}\right]^3 \quad (14)$$

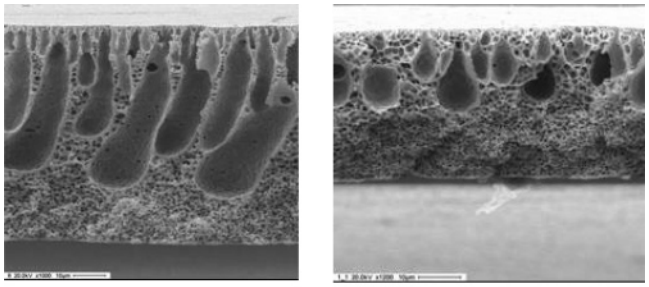

(a) (b)

Figure 5. Cross section of (a) PK membrane (PVDF homopolymer) and (b) PKF membrane (PVDF copolymer).

If $\epsilon = 0$, eq 14 reduces to the form reported in the literature (eq 1) for heterogeneous nucleation on nonporous surfaces.

Materials and Methods

Poly(vinylidene fluoride-*co*-hexafluoropropylene) and poly(vinylidene fluoride) homopolymer were supplied from Elf Autochem under the trade name of Kynarflex 2800 and Kynar 460, respectively. *N*,*N*-Dimethylacetamide (DMA), LiCl, and poly(vinylpyrrolidone) (PVP, MW = 10000) were purchased from Sigma-Aldrich. The casting knife was from Braive Instruments. Cross section and surface morphology of the membranes were examined by a Cambridge Instruments Stereoscan 360 scanning electron microscope (SEM). All the samples were coated with a thin layer of gold before SEM observations. Cross sections have been prepared by fracturing the membrane in liquid nitrogen. Contact angles were measured by CAM 200 contact angle meter (KSV Instruments LTD, Helsinki, Finland). Droplets of distilled water and protein solutions, having a volume of 5 μL, were deposited on the upper surface of the membranes using an automatic microsyringe. The average value and standard deviation of five experiments in different regions of each membrane were determined. Mean pore size and effective porosity (defined as surface porosity over effective pore length) were calculated by gas permeation according to the method described by Wang et al.[16] The experimental equipment used for gas permeation studies was manufactured by GKSS Forschungszentrum GmbH (Germany). Gas permeance of the membranes was tested for pure N_2 gas. Measurements were carried out at 25 ± 1 °C at a series of transmembrane gas pressures ranging from about 100 to 1200 mbar.

Membrane Preparation. Flat sheet porous membranes were prepared by a nonsolvent-induced phase inversion process.[17] Homogeneous solutions were obtained by dissolving in DMA the PVDF polymer pellets (20 wt %) at room temperature by magnetic stirring for about 24 h. After the addition of an appropriate amount of pore forming additive (LiCl or PVP), solutions were again homogenized by stirring. Polymeric solutions were first cast on a glass plate by a hand-casting knife with a gap of 250 μm and then immersed for 2 h in a coagulation bath containing distilled water at 20 ± 2 °C. Films were removed and immersed in another bath of distilled water for additional 24 h and finally washed with ethanol in order to remove residual traces of solvent or additives. Membranes were dried in an oven at 60 °C under vacuum for 24 h.

Membrane Characterization. Membrane morphology was investigated by SEM observation. Porous asymmetric membranes were obtained from both PVDF homopolymer and copolymer (Figure 5); membrane structure and transport properties can be modulated by using an appropriate amount of pores forming additives in the casting solution. A complete discussion of the effect of water-soluble additives on membrane structure goes beyond the scope of this work; more details are reported in ref 18.

TABLE 1: Composition (wt %) of the Casting Solutions, Identification Codes, and Morphological Properties of PVDF Membranes

DMA	LiCl	PVP	ID code	mean pore size (μm)	porosity	thickness (μm)
KYNAR 460 (20 wt %)						
80.0			PK	0.11	4.6×10^{-1}	87.4
77.5	2.5		PK-L2	0.14	5.4×10^{-1}	98.9
75	5.0		PK-L5	0.043	4.4×10^{-1}	103
72.5	7.5		PK-L7	0.056	2.7×10^{-1}	101
77.5		2.5	PK-P2	0.21	4.0×10^{-1}	122
75		5.0	PK-P5	0.20	4.5×10^{-1}	150
72.5		7.5	PK-P7	0.22	5.8×10^{-1}	150
KYNAR FLEX 2800 (20 wt %)						
80.0			PKF	0.034	6.0×10^{-3}	41.4
77.5	2.5		PKF-L2	0.072	4.3×10^{-2}	69.4
75.0	5.0		PKF-L5	0.084	5.9×10^{-1}	117
72.5	7.5		PKF-L7	0.043	3.2×10^{-1}	91.5
77.5		2.5	PKF-P2	0.044	1.1×10^{-1}	103
75		5.0	PKF-P5	0.092	5.4×10^{-1}	121
72.5		7.5	PKF-P7	0.19	2.7×10^{-1}	153

Table 1 summarizes the main structural properties of the different kinds of PVDF membranes prepared: mean pore size, porosity, and thickness. An identification code for each membrane, used in the following part of the paper for convenience, is also reported.

Crystallization Tests. Hen egg with lysozyme from Sigma-Aldrich (HEWL, Product Code L-6876), lyophilized and three times recrystallized, was used without additional purification. The protein was dissolved in 0.05 M sodium acetate buffer at pH 4.5; a precipitant solution was prepared by dissolving an appropriate amount of NaCl (reagent grade) in sodium acetate buffer. Both solutions, prepared using ultrapure water supplied by Millipore (Milli-Q), were filtered and mixed in equal volumes to give a final NaCl concentration of 1.5%, 2%, 2.5%, and 3% w/v and a final protein concentration of 40 mg/mL. The concentration of protein in solution was checked by absorbance measurements at 280 nm by Shimadzu UV-160 recording spectrophotometer.

In a typical crystallization experiment, 25 μL of protein solution was deposited on the surface of a polymeric membrane—previously placed in a crystallization cell (Figure 6)—and kept at 5 °C. Mass transfer was activated by contacting the opposite side of the membrane with 1 mL of stripping solution, consisting of NaCl solution having a w/v concentration double with respect to the precipitant concentration in the protein solution. The membrane surface was observed by optical microscope Axiovert 25 (Zeiss) equipped with a video camera JVC, TK-C1480B. Crystals were scored by number and size every 12 h since their appearance.

Results and Discussion

Analogously to the homogeneous process, heterogeneous nucleation rate (representing the number of nuclei that cross the energy barrier ΔG^*_{het} for critical cluster formation per unit of time) shows a strong nonlinear dependence on the interfacial energy. In addition, our theoretical analysis (and, formally, eq 14) demonstrates that the thermodynamic term $\Delta G^*_{het}/\Delta G^*_{hom}$ is a function both of the surface chemistry of the polymeric membrane and of its porous structure.

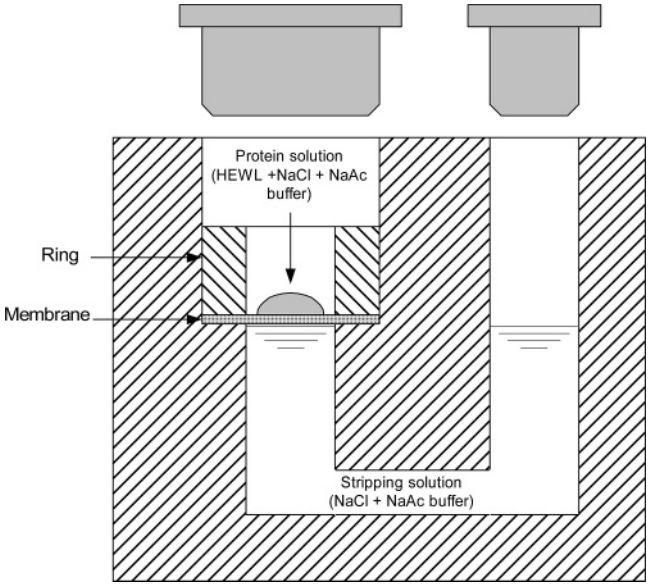

Figure 6. Membrane crystallization cell used in the present work.

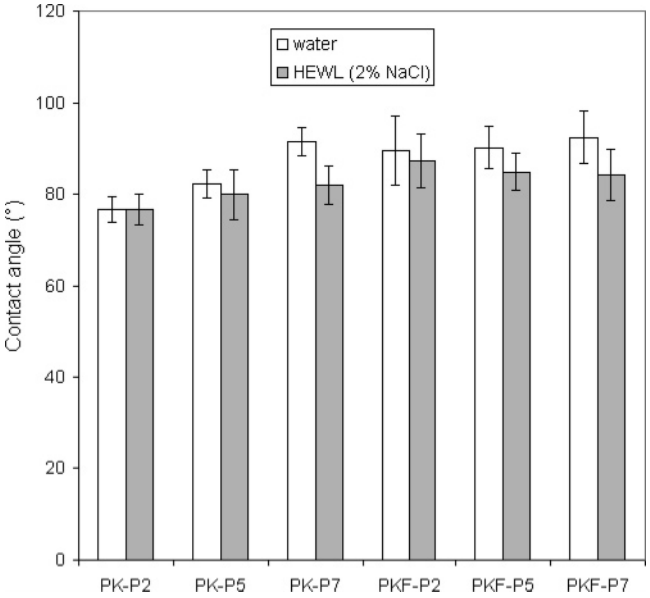

Figure 7. Observed contact angles of water and lysozyme solution (2% w/v NaCl) on PVP-modified PVDF membranes.

In this study, contact angle measurements have been used to correlate free energy for critical nucleus formation to free energies of the interfaces involved. Some of the observed contact angles for water and crystallizing solutions of lysozyme on PVDF membranes are plotted in Figure 7; data roughly scatter around 80°.

With important exceptions, most proteins tend to adsorb more extensively at hydrophobic than at hydrophilic surfaces;[19,20] the behavior of proteins undergoing limited or no interfacial conformational changes (so-called "hard" proteins) follows this expectation. This is the case for reasonably spherical/symmetric proteins such as lysozyme with approximate dimension of 3.0 × 3.0 × 4.5 nm.[21]

Because of the protein absorption on the membrane surface, the hydrophilicity of the porous materials tends to increase, resulting in contact angles lower than those measured using water.[22] Experimental data show that differences among observed contact angles of water and lysozyme solution with NaCl 2% w/v are within 11% for both Kynar and Kynarflex PVDF membranes. The largest discrepancy has been observed on PK-P7 membrane, being contact angles of water and lysozyme solution 91 ± 3° and 82 ± 4°, respectively. An important variation (9.7%) has been also experienced for PKF-P7 membranes; moreover, differences increase at higher amounts of the PVP additive. Similar considerations can be extended to LiCl-modified membranes, although the extent of the gap between contact angles of water and protein solution is generally reduced (<5%).

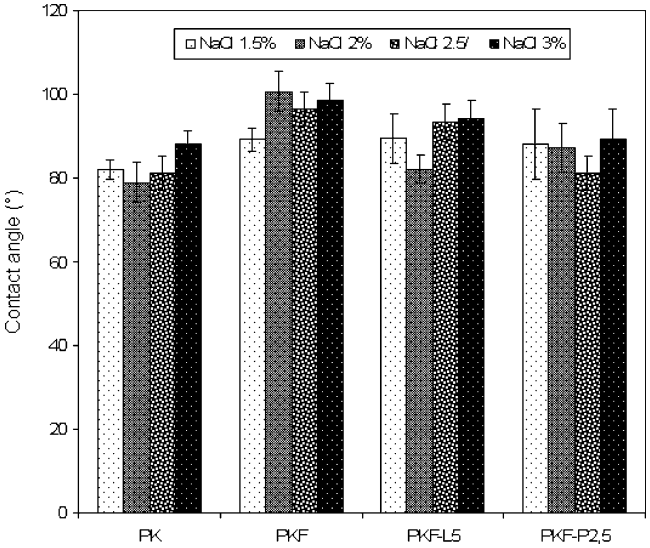

Figure 8. Contact angles of protein solutions at different precipitant concentrations on selected PVDF membranes.

The extent of solution−membrane interactions depends on pH, since molecules change their charged state as a consequence of modifications in their solution environment.

Studying the influence of electrostatic interactions on the adsorption of lysozyme at silica surfaces, Van del Veen and colleagues[23] have observed that the adsorbed amount as a function of pH passes through a maximum at pH 9.8, which is about one pH unit below its isoelectric point (pI). Protein absorption is also affected by the ionic strength. At working pH (in the present study pH< pI) it is expected that at higher ionic strength protein adsorption is depressed at electrostatically attractive conditions, thus leading to increasing contact angles.

However, contact angle data for lysozyme at different precipitant concentrations exhibit a more complicated pattern, shown in Figure 8, thus providing evidence for competition between protein molecules and salt ions.

Because of its dependence on the contact angle, heterogeneous nucleation rate can be controlled by changing the interaction of HEWL solution with the membrane. The maximum of the free energy change associated with cluster formation, corresponding to the energy barrier that nuclei must overcome to become stable, is plotted in Figure 9 at different membrane porosity using eq 14.

Points are located on the graph according to the contact angle measured for a lysozyme solution at 2% w/v NaCl concentration; for all PVDF membranes prepared, contact angles do not exceed 100°. Under the constrains imposed by α values, the effect of porosity appears relevant in the range of interest for this study, and the energetic barrier decreases at higher porosity.

For instance, the predicted $\Delta G_{het}/\Delta G_{hom}$ ratio for PKF-P2 membrane ($\epsilon = 0.11$) is 0.30, 35% lower than the value calculated by eq 1 for an ideal dense polymeric matrix having the same contact angle (87.4 ± 5.8°).

In the case of a low-porosity PKF membrane ($\epsilon = 0.0059$), also characterized by the highest measured contact angle (100

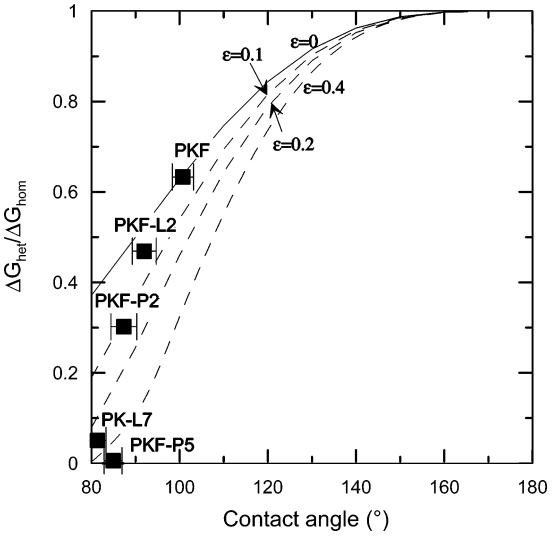

Figure 9. $\Delta G_{het}/\Delta G_{hom}$ ratio as a function of the contact angle of HEWL solution (2% w/v NaCl) at different porosity (lines are from eq 14, symbols are experimental points).

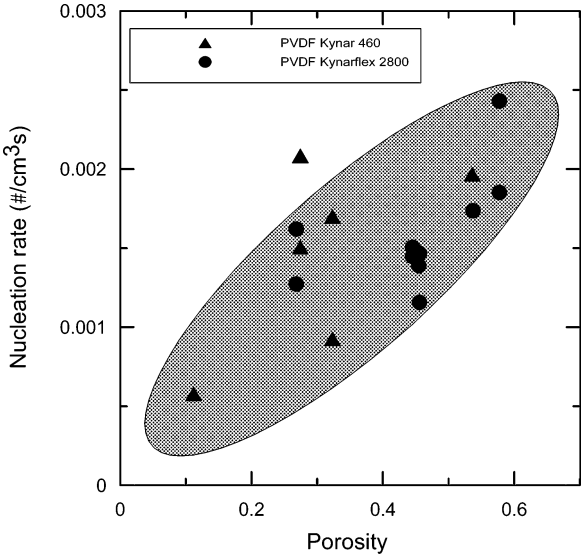

Figure 10. The increasing trend of the HEWL heterogeneous nucleation rate with porosity for modified PVDF Kynar/Kynarflex membranes (precipitant concentration: 2.5−3% w/v).

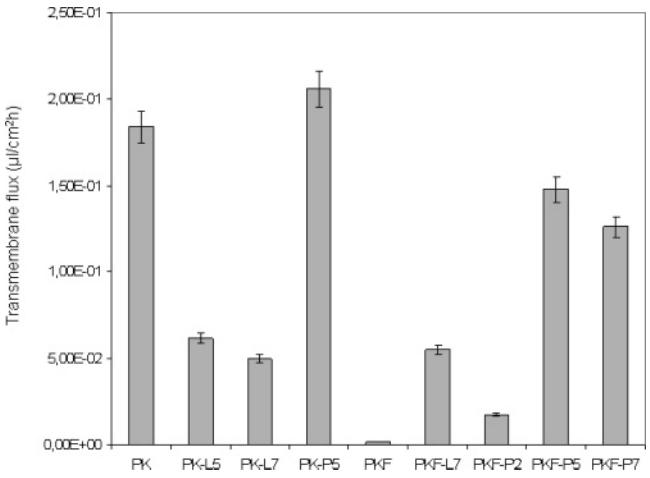

Figure 11. Transmembrane flux measured on PVDF membranes for HEWL protein solution at 3% w/v NaCl.

$\pm$ 2.5°), the ratio $\Delta G_{het}/\Delta G_{hom}$ differs only by 1.5% with respect to the value of 0.64 predicted by the traditional Volmer equation.

Evidence for a favorable effect of porosity with respect to crystallization kinetics is also present in the literature. Luryi and Suhir have observed that the stress energy in the forming crystals is drastically reduced due to pores existing on the substrate surface.[24] The problem of enhanced macromolecular nucleation on a porous silicon surface (PSS) has been theoretically investigated by Stolyarova et al. considering the substrate as a fractal object. It was stated that, although the lattice constant of typical protein crystals (of the order of 10 nm or more) is similar to the pore size of PSS used, pores provide the formation of nuclei for further crystallization on the surface.[25]

In principle, the possibility to correlate the membrane morphology to the kinetics of nucleation might offer the opportunity of a more rationale design of a crystallization process.

The theory−experiment connection has been verified by measuring nucleation rates of lysozyme on membranes characterized by different contact angles and, therefore, different interfacial free energies.

Steady-state nucleation rates have been obtained by determining microscopically the number of crystals generated after 48 h. Kinetic data for various modified PVDF Kynar/Kynarflex membranes characterized by different morphologies, and measured for HEWL solutions with different precipitant concentrations, are cumulatively plotted in Figure 10.

A qualitative increase of the nucleation rate with porosity is seen, in agreement with the tendency of the nucleation barrier ΔG to decrease at higher porosity.

Volmer's theory[7] establishes a linear dependence between the logarithm of the nucleation rate and the second power of the supersaturation, representing the driving force of a crystallization process. Therefore, the rate of solvent removal in vapor phase through a microporous membrane is expected to affect the crystallization kinetics. The transmembrane flux (J) is strictly related to the structural properties of the membrane, including porosity (ϵ), tortuosity (τ), pore size (r), and thickness (δ), according to the dusty gas model equation simplified for the Knudsen-limited diffusion through a porous material[26]

$$J = \frac{2\epsilon r}{3\tau}\frac{1}{RT}\left(\frac{8RT}{\pi M}\right)^{1/2}\frac{\Delta p}{\delta} \qquad (15)$$

where R is the gas constant, T is the temperature, M is the molecular weight, and Δp is the gradient of partial pressure. Figure 11 illustrates data of transmembrane flux for different Kynar and Kynarflex PVDF membranes at 3% NaCl. Within the accuracy limit allowed by preparation procedures, the effect of the membrane porosity can be quantitatively evaluated by comparing PK-L5 and PKF-L7 membranes: both membranes have the same pore size (0.043 μm) and a similar thickness (103 μm for PK-L5, 91.5 μm for PKF-L7). A solvent flux of 5.5×10^{-2} μL/(cm^2 h) is achieved with PKF-L7 membrane having a porosity of 0.32; the flux increases by 12% for a PK-L5 membrane having a porosity of 0.44. The mass transfer rate raises with the membrane pore size, as suggested by the comparison between PK-L5 and PK membranes. In this case, porosities are very close, thicknesses vary of about 17%, and the pore size of the PK membrane is 0.11 μm; the corresponding transmembrane flux at NaCl 3% w/v is 1.8×10^{-1} μL/(cm^{2}h).

In general, experimental observations suggest that, using the same membrane, a high removal rate of the solvent from the crystallizing solution causes the formation of a lot of small crystals, whereas the growth of a few large crystals has been experienced at low transmembrane flux.

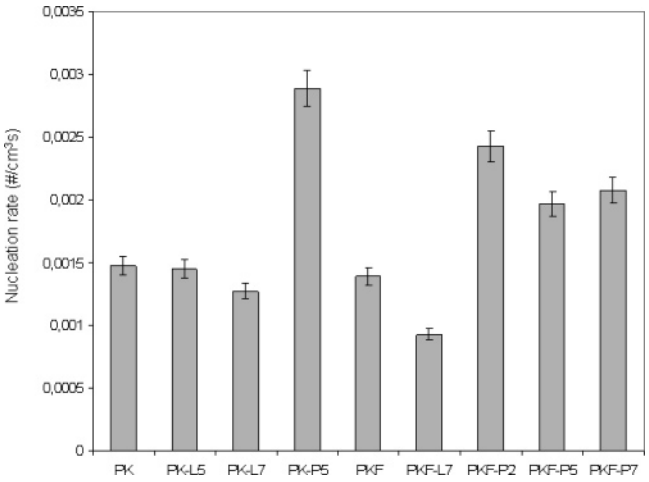

Figure 12. HEWL nucleation rates measured on PVDF membranes at 3% w/v NaCl.

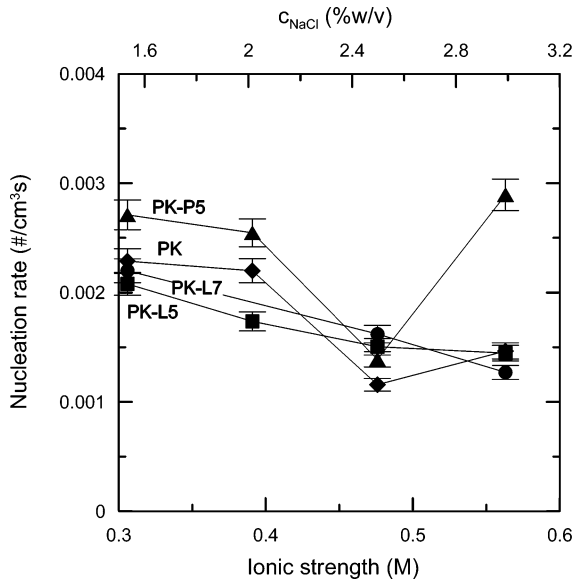

Figure 13. Experimental HEWL nucleation rates on selected PVDF−Kynar membranes as a function of the ionic strength and % NaCl w/v.

As reported in Figure 12, HEWL nucleation rates at 3% w/v NaCl range within 0.9×10^{-3} and 2.9×10^{-3} cm^{-3} s^{-1}, being the highest value measured on the PK-P5 membrane and the lowest one on PKF-L7 membrane.

The critical influence of the transmembrane flux on the nucleation rate is evident if one considers that, under the same crystallization conditions, PK-P5 membrane has the highest solvent removal rate (2.1×10^{-1} μL/(cm^2 h)).

Homogeneous nucleation rates reported by Galkin and Vekilov for lysozyme crystallization carried out at 12.6 °C in 0.05 M acetate buffer pH = 4.5 and 3% w/v NaCl, roughly vary between 10^{-2} and 10^{-1} cm^{-3} s^{-1}.[27] Classical nucleation theory gives explanation for these differences, since a higher temperature enhances the crystallization kinetics up to a maximum in proximity of the liquid−liquid phase boundary hidden below the solubility line in the phase diagram of the protein solution.[28]

The variation of nucleation rate at four different concentrations of NaCl, used both as precipitant in the protein solution and as stripper on the opposite side of the membrane, is reported in Figure 13 for various PVDF Kynar membranes. With the exception of PK-L7 membrane, curves exhibit a minimum in correspondence of a NaCl concentration of 2.5% w/v.

This and other unobvious behaviors of a protein crystallization process seem to be a consequence of the complex interactions between macromolecules in solution (electrostatic and van der Waals forces, hydrogen bonding, hydration, etc.), depending on the physicochemical conditions such as pH, temperature, and composition.

The osmotic second virial coefficient B_{22} provides a measure of the protein−protein pair potential: if B_{22} is positive, the net interaction between protein molecules is repulsive; when B_{22} is negative, the net interaction between protein molecules is attractive. A necessary, but insufficient, requirement for the success of protein crystallization tests is that values of B_{22} vary in a precise range.[29] For lysozyme, B_{22} should be in the interval -2×10^{-4} to -8×10^{-4} mol mL g^{-2}. A progression toward more negative values corresponds to an increase of protein−protein interactions. For B_{22} greater than -2×10^{-4} mol mL g^{-2}, the intermolecular attraction is usually not sufficiently strong to form stable protein crystals. B_{22} lower than -8×10^{-4} mol mL g^{-2} implies protein−protein attractions so strong that the protein molecules may not have adequate time to orient themselves to form a crystalline lattice, some times leading to an amorphous precipitate.

Moreover, a second virial coefficient affects the activity coefficient of the protein solution and, consequently, the transmembrane flux through the membrane.

Literature provides B_{22} values for lysozyme solutions under several crystallization conditions involving sodium acetate buffer and NaCl as precipitant.[30−32] These data, homogenized in terms of ionic strength and interpolated when necessary, are used for discussing results obtained in the present work.

Figure 13 depicts the trend of the nucleation rate against the ionic strength in the protein solution. Although the discussion that follows concerns the PK membrane, it can be generalized for the other membranes reported in the legend.

At a precipitant concentration of 1.5% w/v and 5 °C, B_{22} is -3.5×10^{-4} mol mL g^{-2} and the transmembrane flux reaches its maximum value of 2.5×10^{-1} μL/(cm^2 h). An increase of NaCl content reduces the activity of the protein solution, thus leading to a progressive depletion of the mass transfer driving force. For NaCl 2.5% w/v, B_{22} continues its progression toward more negative values (-6.2×10^{-4} mol mL g^{-2}), the activity coefficient of the crystallizing solution reduces of about 19% and the flux of the vaporized solvent drops off to 2.1×10^{-1} μL/(cm^2 h). The experimental conditions corresponding to the highest precipitant concentration (3% w/v) are characterized by the lowest value of vapor flux (1.8×10^{-1} μL/(cm^2 h)). Up to a ionic strength of 0.48 M, the reduced rate of solvent removal affects the supersaturation level of the solution, and the nucleation rate decreases from 2.3×10^{-3} to 1.1×10^{-3} cm^{-3} s^{-1}. In Figure 13, PK and PK-P5 curves exhibit a minimum in the nucleation rate in correspondence of 2.5% w/v NaCl. At high precipitant concentrations, the PK-L5 kinetic curve gently approaches its lowest value, while the nucleation rate of lysozyme crystals on PK-L7 membrane decreases with almost constant slope.

In most cases, as confirmed also by kinetic data reported in Figure 13, the effect of the transmembrane flux on the nucleation rate is counterbalanced by the enhancement of protein−protein interactions at high precipitant concentrations. As a consequence, the saturation of the protein solution decreases and the crystallization system operates at higher supersaturation levels.

At 5 °C and 1.5% w/v NaCl, the solubility of lysozyme is about 7 mg/mL, but decreases to <1 mg/mL for precipitant concentration greater than 2.5% w/v. The influence on the

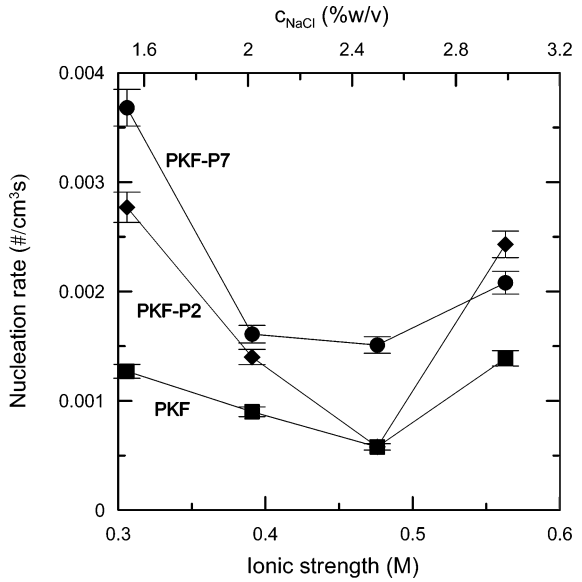

Figure 14. Experimental HEWL nucleation rates on selected PVDF−Kinarflex membranes as a function of the ionic strength and % NaCl w/v.

crystallization kinetics can be drastic; for instance, as the ionic strength increases from 0.48 to 0.56 M, the nucleation rate measured on PK-P5 membranes practically doubles, raising from 1.4×10^{-3} to 2.9×10^{-3} cm^{-3} s^{-1}.

A similar trend in the nucleation rate is reported in Figure 14 for PVDF−Kynarflex membranes, and curves attain a minimum value at 2.5% w/v NaCl.

In correspondence of 2% w/v NaCl, the heterogeneous nucleation rate of lysozyme crystals on unmodified PKF is 0.0009 cm^{-3} s^{-1}, the lowest value observed among the three membranes compared in the diagram at the same precipitant concentration. For this membrane, the calculated $\Delta G_{het}/\Delta G_{hom}$ ratio is 0.63, while the low porosity of the polymeric substrate (5.9×10^{-3}) causes a low transmembrane flux of 2.6×10^{-3} μL/(cm^2 h).

For PKF-P2 membrane, the nucleation rate (0.0014 cm^{-3} s^{-1}) is 55% higher than that for the PKF membrane, in agreement with the lower value of the energetic barrier to the formation of critical clusters ($\Delta G_{het}/\Delta G_{hom} = 0.30$, corresponding to a porosity of 0.11) and with the 1 order of magnitude higher solvent flux through the microporous membrane (2.5×10^{-2} μL/(cm^2 h)).

Nucleation rate is 0.0016 cm^{-3} s^{-1} for PKF-P7 membrane, characterized by a solvent transmembrane flux of 1.9×10^{-1} μL/(cm^2 h) and a $\Delta G_{het}/\Delta G_{hom}$ of about 0.1.

Conclusions

At the moment, the experience in protein crystallization suggests that there is yet no reliable and simple methods of generating high-quality crystals, whereas extensive, often random and always time-consuming screening procedures have to be carried out in order to find suitable crystallization conditions. Microporous membranes, able to promote the epitaxial growth of crystals, seem to have the capability to better control the crystallization kinetics by acting on the structural parameters of these polymeric substrates.

In this work, the influence of membrane porosity on the energetic barrier to nucleation process has been mathematically derived and discussed on the basis of HEWL crystallization experiments carried out on PVDF membranes characterized by different morphologies. It has been also shown that different chemical and physical interactions between hydrophobic membrane and mother liquor, induced by using appropriate modifying molecules (LiCl and PVP) and described in terms of observed contact angles, have important effects on the thermodynamics of the formation of critical nuclei.

Also in agreement with the limited amount of data available in the literature,[14] the theoretical model here proposed explains why the ability of a porous surface to enhance nucleation rate is general and not limited to amphoteric macromolecules absorbed on charged or hydrophobic substrates.

Connection between membrane morphology and transmembrane flux has been emphasized, since it has been experimentally verified that a reduced removal rate of solvent decreases the nucleation rate. This trend, observed at increasing precipitant (NaCl) concentration, is counterbalanced by the reduction of protein solubility; in most cases, this fact causes the appearance of a minimum in the nucleation rate in correspondence of a ionic strength of 0.45−0.5 M.

In conclusion, authors consider that the ability to correlate physicochemical and structural membrane properties to the kinetics of nucleation might offer the opportunity of a more rationale design of a crystallization process.

Acknowledgment. The financial support from the "Ministero dell'Istruzione dell'Università e della Ricerca" (MIUR) (Centre of Excellence CEMIF.CAL-CLAB01TYEF and FIRB CAMERE-RBNE03JCR5) is gratefully acknowledged.

References and Notes

(1) McPherson, A.; Shlichta, P. *Science* **1988**, *230*, 385.
(2) Kimble, W. L.; Paxton, T. E.; Rousseau, R. W.; Sambanis, A. *J. Cryst. Growth* **1998**, *187*, 268.
(3) Fermani, S.; Falini, G.; Minnucci, M.; Ripamonti, A. *J. Cryst. Growth* **2001**, *224*, 327.
(4) Rong, L.; Komatsu, H.; Yoda, S. *J. Cryst. Growth* **2002**, *235*, 489.
(5) Sanjoh, A.; Tsukiharaa, T.; Gorti, S. *J. Cryst. Growth* **2001**, *232*, 618.
(6) Sanjoh, A.; Tsukihara, T. *J. Crystal Growth* **1999**, *196*, 691.
(7) Volmer, M.; Webber, A. *Z. Phys. Chem.* **1925**, *119*, 227.
(8) Rieke, P. C. *J. Cryst. Growth* **1997**, *182*, 472.
(9) Curcio, E.; Di Profio, G.; Drioli, E. *J. Cryst. Growth* **2003**, *247*, 166.
(10) Di Profio, G.; Curcio, E.; Cassetta, A.; Lamba, D.; Drioli, E. *J. Cryst. Growth* **2003**, *257*, 359.
(11) Curcio, E.; Simone, S.; Di Profio, G.; Drioli, E.; Cassetta, A.; Lamba, D. *J. Membr. Sci.* **2005**, *257*, 134.
(12) Di Profio, G.; Curcio, E.; Drioli, E. *J. Struct. Biol.* **2005**, *150*, 41
(13) Di Profio, G.; Perrone, G.; Curcio, E.; Cassetta, A.; Lamba, D.; Drioli, E. *Ind. Eng. Chem. Res.* **2005**, *44*/*26*, 10005.
(14) Stolyarova, S.; El-Bahar, A., Nemirovsky, Y. *J. Cryst. Growth* **2002**, *192*, 237.
(15) Troger, J.; Lunkwitz, K.; Burger, W. *J. Colloid Interface Sci.* **1997**, *194*, 281.
(16) Wang, D.; Li, K.; Teo, W. K. *J. Membr. Sci.* **1999**, *163*, 211.
(17) Kimmerle, K.; Strathmann, H. *Desalination* **1990**, *79*, 283.
(18) Fontananova, E.; Jansen, J. C.; Cristiano, A.; Curcio E.; Drioli, E. *Desalination* **2006**, *192*, 190.
(19) Norde, W. *Adv. Colloid Interface Sci.* **1986**, *25*, 267.
(20) Haynes, C. A.; Norde, W. *Colloids Surf., B* **1994**, *2*, 517.
(21) Malmsten, M. *J. Colloid Interface Sci.* **1998**, *207*, 186.
(22) Palacio, L.; Calvo, J. I.; Pradanos, P.; Hernandez, A.; Vaisanen, P.; Nystrom, M. *J. Membr. Sci.* **1999**, *152*, 189.
(23) van der Veen, M.; Norde, W.; Cohen Stuart, M. *Colloids Surf., B* **2004**, *35*, 33.
(24) Luryi, S.; Suhir, E. *Appl. Phys. Lett.* **1986**, *49*, 140.
(25) Stolyarova, S.; Baskin, E.; Chayen, N. E.; Nemirovsky, Y. *Phys. Status Solidi* **2005**, *8*, 1462.
(26) Datta, R.; Dechapanichkul, S.; Kim, J. S.; Fang, L. Y.; Uehara, H. *J. Membr. Sci.* **1992**, *75*, 245.
(27) Dixit, N. M.; Kulkarni, A. M.; Zukoski, C. F. *Colloids Surf., A* **2001**, *190*, 47.
(28) Galkin, O.; Vekilov, P. G. *J. Cryst. Growth* **2001**, *232*, 63.
(29) George, A.; Wilson, W. W. *Acta Crystallogr., D* **1994**, *50*, 361.
(30) Bonneté, F.; Finet, S.; Tardieu, A. *J. Cryst. Growth* **1999**, *196*, 403.
(31) Rosenbaum, D. F.; Zukoski, C. F. *J. Cryst. Growth* **1996**, *169*, 752.
(32) Gripon, C.; Legrand, L.; Rosenman, I.; Vidal, O.; Robert, M. C.; Boué, F. *J. Cryst. Growth* **1997**, *178*, 575.